General Disclaimer

One or more of the Following Statements may affect this Document

- This document has been reproduced from the best copy furnished by the organizational source. It is being released in the interest of making available as much information as possible.

- This document may contain data, which exceeds the sheet parameters. It was furnished in this condition by the organizational source and is the best copy available.

- This document may contain tone-on-tone or color graphs, charts and/or pictures, which have been reproduced in black and white.

- This document is paginated as submitted by the original source.

- Portions of this document are not fully legible due to the historical nature of some of the material. However, it is the best reproduction available from the original submission.

PRE-RESONANCE RAMAN SPECTRA OF SOME SIMPLE GASES

A FINAL TECHNICAL REPORT

By

Pauline W. Low
Graduate Assistant
Old Dominion University

Under the direction of
Alan R. Bandy
Associate Professor of Chemistry
Old Dominion University

Prepared for the
NATIONAL AERONAUTICS AND SPACE ADMINISTRATION
Langley Research Center
Hampton, Virginia 23665

Under
Research Grant NGR 47-003-049

Submitted by the
Old Dominion University Research Foundation
P.O. Box 6173
Norfolk, Virginia 23508

March 1974

ACKNOWLEDGEMENT

The author would like to express her indebtedness to Dr. Alan Bandy, research director, for his invaluable advice and guidance during this research project. Acknowledgement is also in order to Dr. Robert Ake for many enlightening discussions. Financial assistance during this project was provided by NASA Grant 047-003-049, for which the author is grateful.

ABSTRACT

The pre-resonance Raman spectra of SO_2, N_2O, and H_2S have been investigated using the 4880 Å, 4727Å, and 4579Å lines of the argon ion laser. Although these molecules have electronic absorption bands in the near ultraviolet, none have exhibited any pre-resonance enhancement within our experimental error of $\pm$ 10%. Possible explanations taking into account the current theories for resonance Raman are discussed.

TABLE OF CONTENTS

LIST OF TABLES

LIST OF FIGURES

INTRODUCTION

The Raman effect is the inelastic scattering of light by molecules which results in a frequency difference between the scattered light and incident light. The intensity of scattered light is proportional to the cross section which, under normal conditions far from an electronic absorption band, is dominated by a term containing the fourth power of the frequency of the scattered light. However, when the incident light wavelength approaches or coincides with the wavelength of an electronic absorption band, there can be an enhancement of intensity which is larger than the fourth power of the frequency and is known as the resonance Raman effect. This effect has been observed in several gases as well as liquids and solutions. (1, 2,3,4,5,)

When intensity enhancement occurs with incident light approaching but not entering an electronic absorption band, the effect is known as the pre-resonance Raman effect. In this work a study of the pre-resonance Raman spectra of SO_2, N_2O, and H_2S has been undertaken by measuring the Raman cross sections of these molecules using the 4880Å, 4727Å, and 4579Å lines of the argon ion laser for excitation.

The molecules were chosen primarily because several of their electronic absorption bands fall in the near ultraviolet. Since these electronic absorption bands are not far from the exciting wavelengths used, there should be a high probability of observing some pre-resonance enhancement of the Raman cross sections in these molecules. Because their electronic absorption bands differ in intensity, amount of vibronic structure, band width and band frequency, this study might

provide some information on how these characteristics of the electronic absorption band affect the dependence of the Raman cross section on exciting wavelength.

The electronic absorption spectra in the regions of interest of the three molecules are seen in Figures 1, 2, and 3. Sulfur dioxide (see Figure 1) has three near ultraviolet transitions. A weak band is observed in the 3400-3900 Å region and is assigned to a $^3B_1 \leftarrow {}^1A_1$ forbidden transition.

A medium intensity band is found in the 3000-3400 Å region and is assigned to a $^1B_1 \leftarrow {}^1A_1$ transition while the strong band observed in the region 2350-2000 Å is assigned to a $^1B_2 \leftarrow {}^1A_1$ transition. Recently the vibration-rotation structure of the first two bands has been studied in greater detail (6,7,8). Merer (9) showed that the 000-000 bands at 3880 Å are polarized in the plane of the molecule containing all the atoms of the molecule and perpendicular to the C_2 axis of the molecule. Additionally, they showed that the molecule is a symmetric top in both the ground and in all the excited electronic states. Brand, et. al.(6) confirmed this analysis and determined that the r_o(SO) for the excited state is 1.4926 ± 0.0002 Å and the angle is 126°13'±2'. The $^3B_1$ state appears to be strongly perturbed by a neighboring $^3A_2$ state. In fact, Merer (9) observes that one band at 3520 Å which he assigns to the 201-000 component of the $^3A_2 \leftarrow {}^1A_1$ transition is as strong as any of the bands of the $^3B_1 \leftarrow {}^1A_1$ transition. He attributes this to a spin-orbit interaction that mixes the $^3A_2$ state with the higher singlet levels which is nearly as strong as the interaction that allows the $^3B_1$ levels. He further states that the $^3A_2$ bands are perpendicular bands. The 100 level of the $^3B_1$ state is also strongly perturbed; since the 001 state

lies close enough and has the correct symmetry for Coriolus interaction. Brand (7) adds that the 110-100 bands show vibronic interaction in the K structure and states that the interaction matrix element

$$\langle {}^3B_1 v_1 v_2 v_3 | (\partial H/\partial Q_3)_o Q_3 | {}^3A_2 v_1 v_2 v_3 \rangle$$

must then increase with increasing Δv_1, Δv_2, Δv_3. However, this implies different structures in the $^3B_1$ and $^3A_2$ states for which there is no experimental evidence.

Nitrous oxide, which has a $^1\Sigma_g$ ground state and belongs to the C_∞ symmetry group, is linear with a structure N-N-O as determined by Sponer and Bonner (10). These workers found continuous absorption in the region 2595-3065Å and attributed this to a $^3\pi \leftarrow {}^1A_1$ transition, the $^3\pi$ state leading to a dissociation process at 3065Å yielding $N_2 {}^1\Sigma + O {}^3p$ as products. Nitrous oxide has two vibrations of A_1 symmetry which occur at 1285cm^{-1} and 2224cm^{-1} and are designated ν_1 and ν_2 respectively. The ultraviolet absorption spectrum of N_2O is shown in Figure 2.

The spectrum of H_2S (11) in the region 1600-2100Å is a broad continuum with little discrete structure. There are weak diffuse bands at 1875, 1917, and 2005Å. These transitions have four structures with a separation of approximately 1150cm^{-1} and are assigned to ν_2 of the excited electronic state. This frequency can be compared to 1240 cm^{-1} for ν_2 of the ground state. Ground state H_2S has C_{2v} symmetry with ν_1 of A_1 symmetry occurring at 2611cm^{-1}.

In summary, several theoretical studies of Raman intensity (1, 12, 13, 14, 15) point out that the Raman cross section should increase more rapidly than the classical ν^4 dependence when the exciting frequency approaches an electronic absorption band of the molecule, especially when large amounts of vibronic structure are present in these electronic

absorption bands. Experimental studies of liquids, solutions, and a gas phase study on the halogens by Bernstein (2) have in general substantiated these theoretical predictions. The gas phase work by Bernstein, however, showed resonance Raman only when the electronic absorption band was entered. This experiment has been undertaken in order to ascertain if Bernstein's study was an anomoly, since theoretically, resonance enhancement should take place when the absorption band is approached, or if, for gases, the exciting wavelength must be inside the absorption band. The choice of gases was made on the basis that their electronic absorption bands showed a detectable vibronic structure and thus might exhibit a measurable pre-resonance Raman effect and because gases are of importance in environmental studies.

DISCUSSION OF THEORIES

The total Raman radiant intensity, I_{mn}, for the m,n vibration-rotation transition is related to the incident irradiance, i_o, by the expression

$$I_{mn} = \sigma_{mn} i_o \tag{1}$$

where σ_{mn} is the Raman cross section for this transition. (16) For right angle scattering of a particular polarization produced by exciting light of a particular polarization and for a small collection angle, Ω, the Raman radiant intensity is given by the equation

$$I_{mn} = \frac{d\sigma_{mn}}{d\Omega} \Omega \, i_o \tag{2}$$

Here $d\sigma_{mn}/d\Omega$ is the differential cross section for Raman scattering for this scattering geometry. Murphy et. al. (16) related the differential cross section to the derived polarizability tensor with the following equation

$$\frac{d\sigma_j}{d\Omega} = \left[\frac{(2\pi)^4}{45}\right]\left[\frac{b_j^2(\nu_o - \nu_j)^4}{1 - \exp(-h\nu_j c/kT)}\right] g_j (45\alpha'^2_j + 7\gamma'^2_j) \tag{3}$$

where $b_j = (h/8\pi^2\nu_j c)^{\frac{1}{2}}$, g_j is the degeneracy of the jth vibrational mode and $\gamma_j'^2$ is the anisotropy. This equation and experimental data for depolarization ratios allows calculation of $\alpha_j'^2$. The quantity α_j' can in turn be related to microscopic quantities under pre-resonance or resonance conditions by several theoretical approaches.

Shorygin (12) uses a semi-classical approach in his development of resonance Raman theory by considering the terms in the static polarizability expression as a function of the normal coordinates of the ground electronic state. Albrecht (14), on the other hand, uses a quantum mechanical approach involving the Kramers-Heisenberg dispersion

theory* and sums over the excited states. This method involves perturbation theory and was later modified by Albrecht and Tang (15) where the variation method was applied to find the best energies in the energy denominators. All three methods make important simplifications and have significant similarities and differences.

Shorygin (12) begins with the semi-classical expression for static polarizability for one nuclear configuration

$$\alpha = \frac{z^2}{4\pi^2 c^2 m} \sum_e \frac{f_e}{\nu_e^2 - \nu^2 + i\nu\gamma_e} \tag{4}$$

where f_e is the oscillator strength, ν_e, the frequency of the absorption band maximum in cm^{-1}, γ_e is the attenuation coefficient, the remaining constants have their usual meaning and the summation is over all electronic excitation levels. The first and second derivatives which govern the Raman fundemental and overtone intensities respectively are given in the following equations:

$$\frac{d\alpha}{dQ} = \alpha' = \frac{z^2}{4\pi^2 c^2 m} \sum_e \left[\frac{f_e'}{\nu_e^2 - \nu^2 + i\nu\gamma_e} - \frac{2f_e\nu_e\nu_e'}{(\nu_e^2 - \nu^2 + i\nu\gamma_e)^2} \right] \tag{5}$$

$$\frac{d^2\alpha}{dQ^2} = \alpha'' = \frac{z^2}{4\pi^2 c^2 m} \sum_e \left[\frac{f_e''}{\nu_e^2 - \nu^2 + i\nu\gamma_e} - \frac{4f_e'\nu_e\nu_e' + 2f_e\nu_e\nu_e''}{(\nu_e^2 - \nu^2 + i\nu\gamma_e)^2} \right.$$

$$\left. + \frac{2f_e\nu_e'^2(2\nu_e^2 + \nu^2 + i\nu\gamma_e)}{(\nu_e^2 - \nu^2 + i\nu\gamma_e)^2} \right] \tag{6}$$

In differentiating the expression for the polarizability, it should

* For a discussion of the dispersion equation for molecules see "Comments on the Derivation of the Dispersion Equation for Molecules" by G. P. Barnett and A. C. Albrecht in Raman Spectroscopy Volume 2, H. A. Szymanski ed., Plenum Press New York 1970

be noted that f_e and ν_e are in general functions of the normal coordinates. The term f_e can be replaced by the squares of the matrix elements of the transition dipole moment. Equation (4) can then be written (18)

$$(\alpha_{\rho\rho})_{\kappa\kappa} \propto \sum_r \frac{1}{h} \frac{|(M_\rho)_{\kappa r}|^2}{\nu_{r\kappa} - \nu_o} \tag{7}$$

where $(\alpha_{\rho\rho})_{\kappa\kappa}$ is the polarizability of the ground state κ and $\underline{r}$ is the excited state. Differentiation with respect to the normal coordinate $\underline{Q}$ then gives

$$\frac{d(\alpha_{\rho\rho})_{\kappa\kappa}}{dQ} = \frac{1}{h}\sum_r \left[\frac{2\nu_{r\kappa} d|(M_\rho)_{\kappa r}|^2}{\nu_{r\kappa}^2 - \nu_o^2 \, dQ} - \frac{2(\nu_r^2 + \nu_o^2}{(\nu_r^2 - \nu_o^2)^2} |(M_\rho)_{\kappa r}|^2 \frac{d\nu_{r\kappa}}{dQ} \right] \tag{8}$$

The dependence of both f_e and the transition dipole moment upon the normal coordinate is considered to be linear.

The dependence of ν_e upon normal coordinate Q which involves the derivative $d\nu_e/dQ_o$ is estimated from the potential energy curve of the excited electronic state. This gives the slope of the excited electronic state potential energy curve at the point which corresponds to the ground state equilibrium configuration. In theory $d\nu_e/dQ$ can be positive or negative depending upon the direction of the shift of the potential energy curve of the excited electronic state. If ΔQ is defined as $Q_e - Q_o$, then the slope will be negative for a shift where $\Delta Q = Q_e - Q_o > 0$ and positive for a shift where $\Delta Q = Q_e - Q_o < 0$; this is illustrated graphically below

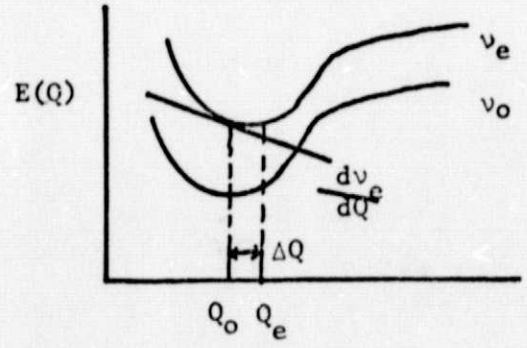

Inspection of equation (5) shows that either the first or second term can be dominant. Where $\nu_e >> \nu_o$ as is the case in most Raman scattering experiments, the first term should dominate, i. e. the ν^4 factor is overriding; however as ν_o increases, as when the exciting frequency approaches an absorption band, the second term becomes dominant and equation (5) can be simplified to

$$|\alpha'| = \frac{z^2 f_e \nu_e \nu_e'}{2\pi^2 c^2 m\left[(\nu_e^2 - \nu^2)^2 + \nu^2\gamma_e^2\right]} \tag{9}$$

Shorygin also points out that since the intensity depends upon the change in the normal coordinates from the equilibrium configuration that the vibrations with the greatest ΔQ will exhibit the strongest Raman intensity. Then the intensity of the stretching vibrations which produce the greatest normal coordinate displacement should increase in intensity more rapidly than other modes when approaching the region of resonance. This in turn implies that $d\nu_e/dQ$ will increase in value also which leads to enhancement of the value of the second term in equation (5).

Albrecht (14) begins the presentation of his quantum mechanical theory with the equation for the radiant intensity of scattered light over a 4π solid angle

$$I_{mn} = \frac{2^7\pi^4}{3^2c^4} I_o (\nu_o + \nu_{mn})^4 \sum_{\sigma\rho} \left|(\alpha_{\rho\sigma})_{mn}\right|^2 \tag{10}$$

where ρ and σ are the Cartesian coordinates of a molecule-fixed system. Using dispersion theory, the $\rho\sigma$th polarizability matrix element for an m-n transition is given by the following equation

$$(\alpha_{\rho\sigma})_{mn} = \frac{1}{h} \sum_r \left[\frac{(M_\rho)_{rn}(M_\sigma)_{mr}}{\nu_{rm} - \nu_o} + \frac{(M_\rho)_{mr}(M_\sigma)_{rn}}{\nu_{rn} + \nu_o}\right] \tag{11}$$

with the sum over all vibronic states of the molecule and

$$(M_\rho)_{mr} = \langle \Psi_r | \vec{m}_\rho | \Psi_m \rangle \tag{12}$$

where Ψ_r and Ψ_m are vibronic wave functions and $\vec{m}_\rho$ is the ρth component of the electric dipole moment operator.

The Born-Oppenheimer approximation which separates the vibronic state into electronic and vibrational states is introduced. In addition the energy of all the vibrational levels is considered constant over a given electronic level. Equation (11) is then summed exclusive of the ground electronic state, since its energy is much less than the excited state energies. Equation (12) can now be written

$$(M_\rho)_{gi,\ ev} = \langle \Theta_e \phi_v^e | \vec{m}_\rho | \Theta_g \phi_i^g \rangle \tag{13}$$

The electronic transition moment at nuclear configuration Q is given by

$$\left[M_\rho (Q) \right]_{ge} = \langle \Theta_e | \vec{m}_\rho | \Theta_g \rangle \tag{14}$$

where Θ_e and Θ_g are electronic wave functions. Instead of expanding $\left[M_\rho (Q)\right]_{ge}$ in a Taylor's series, Albrecht formulates the theory in first order perturbation theory where

$$M_{ge} = M^o_{ge} + \sum_s \lambda_{es}(Q)\, M^o_{gs} \tag{15}$$

and

$$\lambda_{es}(Q) = \left(\sum_a h^a_{es} Q_a \right) \Delta E^o_{es}{}^{-1} \tag{16}$$

Then equation (13) becomes

$$(M_\rho)_{gi,\ ev} = (M_\rho)^o_{ge}(ev|gi) + \sum_{sa} h^a_{es} (\Delta E^o_{es})^{-1} (M_\rho)^o_{gs}(ev|Q_a|gi) \tag{17}$$

where M^o_{ge} is the electronic transition moment to state s evaluated

for the ground state equilibrium configuration and the sum extends over all excited electronic states but e. The equation is over all normal modes and Q_a is the displacement of the ath normal mode and h^a_{es} is a perturbation energy per unit displacement of the ath normal mode due to mixing of the ground state equilibrium configuration and electronic states e and s under vibrational perturbation. The same approach is used for the remaining transition moments so that equation (11) can be written

$$(\alpha_{\rho\sigma})_{gi,\,gj} = A + B + C \tag{18}$$

For ordinary Raman where $\nu_{eg,\,gi} >> \nu_o$, $\nu_{e,g}$ is replaced by ν_e which permits employment of Van Vleck's sum rule with the following results

$$\sum_v (gi|ev)(ev|gj) = (gi|gj) = \delta_{ij} \qquad \text{(Rayleigh scattering)} \tag{19}$$

$$\sum_v (gi|ev)(ev|Q_a|gj) = \sum_v (gj|ev)(ev|Q_a|gi)$$

$$= (gi|Q_a|gj) = \begin{bmatrix} 0 \text{ if } v_a^j = v_a^i \pm 1 \\ \left[(v_a^j + 1)/2\gamma_a\right]^{1/2} \text{ if } v_a^j = v_a^i + 1 \\ (v_a^i/2\gamma_a)^{1/2} \text{ if } v_a^j = v_a^i - 1 \end{bmatrix} \tag{20}$$

where

$$\gamma_a = (4\pi^2 \nu_a/h)$$

For equation (18) then the A term predicts Rayleigh scattering and the B and C terms predict Raman scattering. These expressions are the selection rules for vibrational Raman. There is a further requirement: the electronic states e and s must both be upper states in the allowed electronic transitions. Thus for a totally symmetric ground state the symmetries of s and e must correspond separately to the same symmetry as at least one of the transitions. This requirement incorporates the Raman selection rules. Yet another condition appears in Albrecht's treatment: the normal modes most

highly involved in producing intensity in forbidden transitions show the greatest activity in Raman scattering.

For resonance conditions Albrecht modifies his original equation and includes a damping constant. The resulting equation is very similar to the result obtained by Shorygin. The sum rule can no longer be employed, since the frequency denominator is now involved in the sum. Some interesting differences in the A and B terms from the same terms in ordinary Raman effect are now apparent. If the vibrational wavefunction of the ground and e electronic state are not solutions to the same Schrodinger equation, the A term can also produce Raman; i. e. with $i \neq j$ $(gi|ev)(ev|gj)$ does not necessarily vanish. Conversely, the B term quite possibly will produce Rayleigh scattering since $(gi|Q_a|ev)(ev|gj)$ and $(gi|ev)(ev|Q_a|gj)$ are no longer required to vanish when $i = j$. The B term is given by

$$B = \frac{-1}{h^2} \sum_{v} \sum_{sa} \sum h^a_{es} \left[\frac{(M_\rho)^o_{ge} (M_\sigma)^o_{gs} (gj|ev)(ev|Q_a|gi) + (M_\sigma)^o_{ge} (M_\rho)^o_{gs} (gi|ev)(ev|Q_a|gj)}{(\nu_{ev,gi} - \nu_o + i\gamma_e)(\nu_s - \nu_e)} \right] \tag{21}$$

The B term near resonance can be responsible for a variation in intensities different from the B term in non-resonance Raman. Albrecht points out that vibrations which mix the lowest allowed electronic transition with another allowed transition will increase in intensity relative to all others as resonance is approached.

Albrecht and Tang (15) modified Albrecht's original paper by making an attempt to avoid the adiabatic approximation for excited electronic states. The authors start with Van Vleck's formulation of the $(\alpha_{\rho\sigma})_{mn}$th component of the polarizability

$$(\alpha_{\rho\sigma})_{mn} = \sum_e \left[\frac{\langle m|M_\sigma|e\rangle\langle e|M_\rho|n\rangle}{E_e - E_m - E_o} + \frac{\langle m|M_\rho|e\rangle\langle e|M_\sigma|n\rangle}{E_e - E_n + E_o} \right] \tag{22}$$

where m, n, and e are initial, final and intermediate vibronic states with eigenvalues E_m, E_n, and E_e and eigenfunctions $|m\rangle$, $|n\rangle$, and $|e\rangle$ for the total Hamiltonian $H(r,Q)$. The sum is over e, the complete set of vibronic states. When the adiabatic approximation is applied for vibronic states m and n, the wavefunctions become

$$\Psi_m(r,Q) = \psi_g(r,Q)\mu_i(Q) \tag{23}$$

$$\Psi_n(r,Q) = \psi_g(r,Q)\mu_j(Q) \tag{24}$$

Substitution then gives

$$(\alpha_{\rho\sigma})_{gi,\,gj} = \left\langle i \left| \sum_e \left[\frac{(g|M_\sigma|e)(e|M_\rho|g)}{E_e - E_{gi} - E_o} + \frac{(g|M_\rho|e)(e|M_\sigma|g)}{E_e - E_{gj} + E_o} \right] \right| j \right\rangle \tag{25}$$

or

$$(\alpha_{\rho\sigma})_{gi,\,gj} = \langle i | \alpha_{\rho\sigma}(Q) | j \rangle \tag{26}$$

where integration is over the electronic coordinates only. Then $\alpha_{\rho\sigma}(Q)$ is expanded in a Taylor's series.

$$\alpha_{\rho\sigma}(Q) = \alpha^o_{\rho\sigma}(Q_o) + \sum_a \left[\frac{d\alpha}{dQ}\right]_{Q_o} (Q_a - Q_o) + \tfrac{1}{2}\sum_a \sum_b \ldots . \tag{27}$$

Rayleigh scattering — Raman fundamentals — Raman overtones

However, instead of the previous manipulations, the denominators of equation (25) are expanded in a power series around an average energy, E_{av}. Then

$$\alpha_{\rho\sigma}(Q) = \sum_{N=0}^{\infty}\sum_e (-1)^N \left[\frac{(g|M_\sigma|e)(e|M_\rho|g)(E_e - E_{av})^N}{(E_{av} - E_{gi} - E_o)^{N+1}} + \right. \tag{28}$$

$$\left. \frac{(g|M_\rho|e)(e|M_\sigma|g)(E_e - E_{av})^N}{(E_{av} - E_{gj} + E_o)^{N+1}} \right]$$

where E_e is still an eigenvalue and $|e\rangle$ an eigenfunction of the total Hamiltonian $\underline{H}$. This also implies the denominators are constant in the sum over $\underline{e}$ and the numerators are matrix elements. The result then is

$$\alpha_{\rho\sigma}(Q) = \sum_{N=0}^{\infty} (-1)^N \left\{ \frac{(g|M_\sigma|(H - E_{av})^N M_\rho|g)}{(E_{av} - E_{gi} - E_o)^{N+1}} + \frac{(g|M_\rho(H - E_{av})^N M_\sigma|g)}{(E_{av} - E_{gi} + E_o)^{N+1}} \right\} \quad (29)$$

The above equation is a series expansion of the ground state instead of a sum over electronic states. Such an expression can be differentiated to obtain the polarizability derivatives. It is assumed that the value assigned to E_{av} is a nearly correct one. When the nuclear coordinates are those of the ground state configuration then the above equation is an expression for the ground state polarizabil

Thus while Shorygin (12) considers only one excited state and the symmetric normal mode, Albrecht and Tang (15) consider all vibronic levels. Shorygin (12) points out that the f_e' is the dominant factor for near resonance while Albrecht (14) considers vibronically active normal modes and points out that these should show a great increase in intensity as the absorption band is approached. Equations (8) and (11) of Shorygin and Albrecht respectively, have some interesting similarities (14). The h_{es}^a of Albrecht's theory corresponds to $d\nu_e/dQ$ in Shorygin's theory; in a qualitative way, both represent a change of electronic energy per displacement of the normal coordinate. For Shorygin's equation near resonance and with the sum over $\underline{r}$ dropped

$$I \propto \nu_o^4 \, (\nu_e^2 + \nu_o^2)^2/(\nu_e^2 - \nu_o^2)^4 \quad (30)$$

This predicted frequency dependence has been proven in general to be experimentally successful .

If equation (21) in Albrecht's formulation is considered then

$$I \propto \nu_o^4 \, (\nu_e \nu_s + \nu_o^2)^2 / \, (\nu_e^2 - \nu_o^2)(\nu_s^2 - \nu_o^2)^2 \qquad (31)$$

When $\nu_s \to \nu_e$, the theories predict the same ν_o dependence. However, when $\nu_s >> \nu_e$ Albrecht's equation becomes

$$I \propto \nu_o^4 / (\nu_e^2 - \nu_o^2)^2 \qquad (32)$$

This theory predicts a range of behavior dependent upon the relative positions of ν_e and ν_s at least near resonance.

Finally then although both theories predict an intensity enhancement as the absorption band is approached, Albrecht's theory diverges from Shorygin's when $\nu_s >> \nu_e$.

EXPERIMENTAL

Optical System

The optical system shown in Figure 4 included a Coherent Radiation Model 52C-UV argon ion laser, a halfwave plate, a Jarrell-Ash sample chamber with a focusing lens that focused the laser light in an off-axis resonator multipass system. The Raman scattering was then collected at right angles with a 125mm focal length achromat that focused the Raman signal into a Spex double monochromator. The detection system contained a Centronics P4249BA photomultiplier and SSR photon counting equipment which output the signal on an Esterline strip chart recorder.

This optical system was a modification of the original design which had the laser at a 90^{o} angle to the sample chamber. The present system improved the alignment procedure by eliminating a 45^{o} angle mirror necessary to divert the laser beam into the sample chamber and two 90^{o} angle mirrors that directed the beam into the focusing lens. The path length of the beam was also decreased. This fact, while not critical in the visible region, was very important for ultraviolet excitation since absorption and scattering of the laser beam became a prime liability in that region. Originally this experiment was to include data using the two Ar^{+2} ultraviolet lines at 3511Å and 3638Å. However, the experimental difficulties were formidable and in the long run too time consuming for completion of that phase of the work. The major difficulty of this particular part of the experiment was the necessity of having every component of the system operating at maximum efficiency. Even though most of the technical difficulties had been

overcome, the low power output of the laser on these two lines proved to be the major obstacle in obtaining experimental data.

The excitation line from the laser was passed through a half wave plate A in order to orient the polarization properly, then was focused with a quartz lens B. This lens focused the multipassed laser line at a height of 10 inches from the base of the sample chamber. The light from B was then reflected into the multipass system by mirror C. The multipass system consisted of two parabolic mirrors which produced an off-axis resonator. The light from C was reflected to the upper parabolic mirror D. It in turn reflected the light onto the lower parabolic mirror E and the light was passed in a similar manner approximately twenty times. At the focal point in the multipass system the beam was no more than 3mm in width. Since Raman scattering is over all angles a spherical mirror F was placed at 180° from the collection optic so that the Raman scattering collected was doubled. Focusing lens G focused the scattered radiation on the monochromator slit. The glass slide H was set in the laser beam at approximately Brewster's angle to divert a sufficient amount of radiation to monitor the laser power. The power was recorded by a Coherent Radiation power meter and read in millivolts on a Heathkit multimeter. The laser power varied from almost one watt for 4880Å to less than 50 mW for the 4727Å line. The slits were kept constant at 600 microns for all samples.

The sample was contained in a fluorescence free quartz cell three inches long and one inch in diameter with Brewster angle windows. The cell was positioned so that the laser was focused approximately in its center, although this was not critical. It was important, however, that the cell be positioned so the maximum number of passes hit the

Brewster angle windows and passed on through the cell without hitting the sides of the cell. See Figure 5.

Gas Handling System

The gases were introduced into the sample cell by means of a simple gas transfer line shown in Figure 6. The calibration gases and sample gases were attached to outlets A, B, C, and D. The gases were purified by low temperature distillation. The pressure was read on an open end mercury manometer. All gas pressures were approximately one atmosphere so small leaks in the vacuum system could be tolerated without serious error in pressure measurement.

The sample cell was connected to the vacuum system by means of ¼" stainless steel tubing. The arrangement was such that after initial alignment of the gas cell the gases could be pumped in and out of the system without disturbing the position of the cell. The system was flushed with nitrogen several time between sample gases to insure minimum contamination. After each flushing the system was then evacuated.

Collection of Data

The gases were introduced into the vacuum system after the system was pumped down. The evacuated cell was cut off so the gases were put only in the main line, then frozen out with liquid nitrogen and vacuum distilled. The sample cell was then opened and the gases allowed to expand into the cell and the pressure read on the mercury manometer. The pressure was also read after each completed total scan of the gas to ensure there was no leakage.

A calibration for each laser line was run using O_2, N_2, CH_4, and Freon 22. In each case the ν_1 symmetric stretch was monitored. Each

peak was scanned four times for signal averaging, two forward and two backward.

After the calibrations were completed, the gases under investigation were run. Each gas run was followed by a nitrogen scan to be used for the relative measurement.

The samples were run in two different ways to check reproducibility of results. In the first method each gas was run at all laser exciting lines, then pumped out and nitrogen introduced and run in the same manner. This was repeated for each gas, although in come cases methane was substituted for nitrogen because of its stronger scattering. As previously stated, all lines were scanned four times. In the second method, each gas was run at one wavelength, then pumped out and the reference gas put in. All gases were run with one exciting line until all were done. Then the exciting line was changed and the procedure repeated. The results from both methods were identical within experimental error.

TREATMENT OF DATA

Calibration Curves

Since the calculation of absolute Raman cross sections is extremely tedious and not the principal goal of this research, only the cross sections relative to nitrogen were calculated. The cross section of a molecule calculated experimentally involves several parameters of the optical system itself along with the parameters of the molecule in question.

However, in this case where only a ratio has been calculated it is necessary only to obtain an efficiency curve for the entire optical system calibrated to wavelength instead of an absolute value for each optical component.

The Raman signal and incident intensity are related (17) to the cross section experimentally by:

$$I_R = \left[\int_{\Omega_c}\left(\frac{d\sigma}{d\Omega}\right)d\Omega\right]\frac{I_o}{A}nV \tag{33}$$

where the integration is over the solid angle of collection, n is the density of the scattering centers, V/A is the length from which the photons are collected, I_o is the laser intensity and I_R the Raman intensity. For the differential scattering cross section at 90^o the following approximation can be made with not more than 5% error

$$\left(\frac{d\sigma}{d\Omega}\right) \simeq \frac{1}{\Omega_c}\int_{\Omega_c}\left(\frac{d\sigma}{d\Omega}\right)d\Omega \tag{34}$$

then

$$\frac{d\sigma}{d\Omega} = \frac{I_R}{\Omega_c nLI_o} \tag{35}$$

With photon counting the number of counts observed is related to the Raman signal, I_R, by

$$N_c = \eta F_c I_R \tag{36}$$

where η is the response of the spectrometer and F_c is the ratio of the number of photons entering the slits to the total number scattered into the collection angle, which is approximately one for wide slits.

The quantity Ω_c can be related to experimental parameters by

$$\Omega_c L = M\Omega_m H \tag{37}$$

where Ω_m is the monochromator solid angle, H is the entrance slit height and M, the magnification. Then the scattering cross section in terms of experimental parameters is given by

$$\frac{d\sigma}{d\Omega} = \frac{N_c}{F_c M \Omega_m H n I_o} \tag{38}$$

If the experimental parameters are held constant, a ratio of two cross sections would be

$$\frac{\text{cross section 1}}{\text{cross section 2}} = \frac{N_c/\eta_1 F_c M \Omega_m H n_1 I_{o1}}{N_c/\eta_2 F_c M \Omega_m H n_2 I_{o2}} \tag{39}$$

where all the optical parameters would cancel except η_1 and η_2, the response, since it is also a function of wavelength. This would give then

$$\frac{\text{cross section 1}}{\text{cross section 2}} = \frac{N_{c1}/\eta_1 n_1 I_{o1}}{N_{c2}/\eta_2 n_2 I_{o2}} \tag{40}$$

Taking this equation and rearranging and substituting σ_1 and σ_2 for cross section 1 and cross section 2 respectively

$$\frac{\eta_1}{\eta 2} = \frac{N_{c1}/I_o n_1 \sigma 1}{N_{c2}/I O n_2 \sigma 2} \tag{41}$$

where the following proportionalities hold

$$\eta_1 \propto N_{c1}/I_{o1}n_1\sigma_1 \tag{42}$$

$$\eta_2 \propto N_{c2}/I_{o2}n_2\sigma_2 \tag{43}$$

In order to plot the calibration another factor, the so-called "ν^4 law", must be taken into account. This is necessary since the Raman shifts of the calibration gases differ considerably and the wavelength dependence of the scattering must not be included in the calibration curve. Then

$$\eta_1 \propto N_{c1}\lambda_{R1}^4/I_o n_1\sigma_1 \tag{44}$$

$$\eta_2 \propto N_{c2}\lambda_{R2}^4/I_o n_2\sigma_2 \tag{45}$$

The plots are then made for η_2/η_1 verses η_1 where η_1 is calculated for N_2 at the Raman shift for each excitation line. The quantity η_2/η_1 is called $E(\lambda)$, the efficiency of the optical system. The calibration curves for the three excitation lines can be seen in Figures 7, 8, and 9.

The efficiencies for the 4880Å and 4727Å lines (shown in Figures 7 and 8) are straight lines with a negative slope, i. e. the efficiency is increased as the wavelength decreases. However, for the 4579Å line the efficiency is no longer a straight line, but a curve which has a maximum, then decreases as the wavelength decreases. Since the efficiency takes into account the efficiency of the grating and the sensitivity of the photomultiplier as well as other components, a graph of their relative efficiencies as a function of wavelength is shown in Figure 10. If the two curves are combined, the result is a straight line for wavelengths down to approximately 4900Å. However, then the photomultiplier sensitivity reaches a maximum and begins to decrease. Thus while the efficiency curves of the 4880Å and 4727Å

exciting wavelengths fall on the increasing side of both the photomultiplier sensitivity and the grating efficiency, the efficiency curve for the 4579Å line hits a maximum and then a decrease in the photomultiplier sensitivity for a net decrease in sensitivity at the lower wavelengths.

Originally a calibration for the entire region of interest, using all laser excitation lines was plotted. However, it was discovered that the halfwave plate, which was coated for the 4880Å line, depolarized all other lines to an indefinite extent. This made it necessary to calibrate each excitation line separately.

The calibration gases chosen, that is O_2, N_2, CH_4 and CHF_2Cl, all have known cross sections and electronic absorption bands far from the excitation lines used. Additionally, the vibrational bands of the gases monitored were all ν_1, highly polarized bands. The depolarization effects, therefore, were not significant.

Calculation of Cross Sections

After the calibration curves were plotted, the value of $E(\lambda)$ could be read from the graph for each of the gases run and at each excitation line. Since each gas was run with either N_2 or CH_4 as a standard, the cross section was readily calculated from the experimental data. If

$$E(\lambda) = \eta_2/\eta_1 \tag{46}$$

where η_1 is calculated for N_2, then

$$E(\lambda)\eta_1 = \eta_2 \tag{47}$$

but

$$\eta_2 = N_{c2}\lambda_R^4/I_o n_2 \sigma_2 \tag{48}$$

and

$$E(\lambda)_1 = N_{c2}\lambda_R^4/I_o n_2 \sigma_2 \tag{49}$$

The only unknown quantity in the above equation is σ_2 and it is easily calculated. The Raman intensities were measured with a plainmeter, each peak was measured four times and the average taken. In the scans

of the Raman shifts each peak was scanned four times and each one divided by the laser power and the average taken as N_c/I_o.

The results of these calculations are listed in Table 1. Within experimental error the cross sections do not change as the excitation line approaches the electronic absorption band.

DISCUSSION

Qualitatively, the resonance Raman theory predicts intensity enhancement for the Raman bands when the exciting frequency approaches an electronic absorption band of the molecule in question. This enhancement has a positive deviation from the ν^4 law which is

$$I_{mn} = \frac{2^7\pi^5}{3^2c^4} I_o \nu^4 \sum_{\rho\sigma} |\alpha_{\rho\sigma,mn}|^2 \tag{50}$$

Where the exciting line is far from any electronic absorption, the ν^4 is the overriding factor, since the $\alpha_{\rho\sigma,mn}$ remains essentially constant. However, when an electronic absorption band is approached, the $\alpha_{\rho\sigma,mn}$ increases and finally becomes more important than the ν^4.

Experimentally then, one might see little or no intensity enhancement for N_2O or H_2S whose electronic absorption bands lie in the lower near ultraviolet region. However, SO_2 with an absorption band around 3880Å, should show at least some positive deviation from ν^4 although presumably not achieve maximum intensity until the absorption band has been entered or at least closely approached i. e. around 4000Å.

In this present experiment no pre-resonance was found for N_2O or H_2S, and in view of the remoteness of their electronic absorption bands from the lowest exciting wavelength used (4579Å) the result was not surprising. However, SO_2 with a band at 3880Å was expected to show some pre-resonance intensity enhancement. This was not the case.

According to previous experimental data (1), some pre-resonance intensity enhancement should be seen at approximately 4,000 cm^{-1}

from the electronic absorption band. The calculations of these frequencies are seen in Table 2 where ν_{eg} is the electronic absorption band maximum in cm^{-1} and ν_o is the laser frequency, also in cm^{-1}. It can be seen that the values for N_2O and H_2S are much greater than $4{,}000cm^{-1}$, but for SO_2 the value lies in the proper range. Additionally, since theory shows that a_1 bands generally have the strongest intensity enhancement (1, 12, 13, 14, 15) the ν_1 band, which is the a_1 symmetric stretch of SO_2 was the band monitored. Since superficially the experimental conditions necessary to observe pre-resonance enhancement have been met, additional factors, perhaps involving the particular electronic transition, must have an essential influence.

Most of the previous experimental data concerned with pre-resonance effect was acquired from ring compounds; i.e., aromatic molecules. In these compounds the allowed transitions all involve the in-plane modes and are, in general, of A_1 symmetry. However, with SO_2 this is not the case. Application of group theory to SO_2 gives the results shown in Table 3. Since the ν_1 band has the polarizability component α_{zz} while the $^3B_1 \leftarrow {}^1A_1$ electronic transition has the transition moment $|\mu_x|$ these would not couple as strongly as $\nu_3(b_1)$ perpendicular band which has the polarizability component α_{xz}. Additionally, the a_1 band is parallel while the electronic transition is perpendicular. Perhaps in view of this the ν_3 band would show the resonance enhancement that the ν_1 band failed to show. While admittedly a simplistic view, it does correctly reflect the experimental evidence. Behringer (1), using a different approach to what was essentially Shorygin's semi-classical model suggested calculating effective absorption frequencies by using

$$f(0) = \frac{2}{h} \frac{\nu_{eg}}{(\nu_{eg}^2 - \nu_o^2)^2} \tag{51}$$

$$\frac{df}{dQ_o} = \frac{-2}{h} \frac{\nu_{eg}^2 - \nu_o^2}{(\nu_{eg}^2 - \nu_o^2)^2} \nu'_{eg} \tag{52}$$

and by incorporating with these equations the intensity dependence on ν_o to give

$$I_{mn} \propto (\nu_o - \nu)^4 / (\nu_{eg}^2 - \nu_o^2)^2 \tag{53}$$

$$I_{mn} \propto (\nu_o - \nu)^4 (\nu_{eg}^2 + \nu_o^2)^2 / (\nu_{eg}^2 - \nu_o^2)^4 \tag{54}$$

This approach has been at least partially successful in fitting experimental data to the theory. Calculations of the following are seen in Table 4: the ratios of the experimental cross sections for 4880Å/4579Å, the ratio of ν^4 for the same two lines and the same ratios for SO_2 using equations(53)and(54) assuming ν_{eg} to be 3880Å. The ratios of the experimental cross sections are in agreement within experimental error with the ratios of the fourth power of the Raman frequencies. This shows essentially no deviation from the "ν^4 law". When using equation (53)the results are also in fair agreement with the experimental values. However, the results for equation (54) have a deviation that is larger than expected for experimental error which seems to lend support to Behringer's suggestion that there could be absorption bands that are non-active for resonance Raman. Although the calculation involves gross simplifications, it does seem to point to this possibility.

Bernstein, (3) while investigating the halogens, found resonance Raman in all the halogens except Cl_2. However, Cl_2 was the only halogen not excited directly into the long wavelength side of its

absorption band. Indeed, as seen in Table 2 $\nu_{eg}^2 - \nu_o^2$ is small enough for resonance enhancement to occur. Perhaps then, at least for simple gases, pre-resonance enhancement does not occur or occurs only weakly and that for a full resonance Raman effect the excitation line must correspond nearly precisely with the correct vibronic frequency.

A more definitive test of the theories of the pre-resonance and resonance Raman effect for SO_2 would most certainly involve excitation in the ultraviolet region. In Brand's study (8) of the $^3B_1 \leftarrow {}^1A_1$ transition the 200-000 band was placed at 3633Å which is only 5Å away from the 3638Å line of the argon ion laser. Additionally, the 300-000 band is placed at 3550Å, only 19Å away from the 3511Å line. Excitation at these wavelengths then should, if the theory is correct, meet all necessary and sufficient conditions for resonance Raman to occur. These conditions are: a highly structured electronic transition, bands mentioned above among the most intense (see Figure 1), and the ν_1 band of a_1 symmetry, predicted by all theories to show the most intense scattering. In the excited state, $^3B_1$, the ν_1 vibration is shifted from its 1151 cm^{-1} position in the ground state to 718 cm^{-1}, the difference in frequency shift presenting a good test of the state observed in the resonance Raman effect.

It must be pointed out that although excitation in the ultraviolet, especially at the mentioned wavelength, would constitute an excellent test of current theories of the resonance, it in general would not add to the verification of any pre-resonance theories. That is, what exactly happens as the absorption band is approached, but not entered? For this case exciting wavelengths should ideally begin where this experiment ended--at 4579Å and work progressively to lower wavelengths until the electronic band is entered.

FIGURE 1

ELECTRONIC ABSORPTION OF SO_2 AT 3400-3900Å *

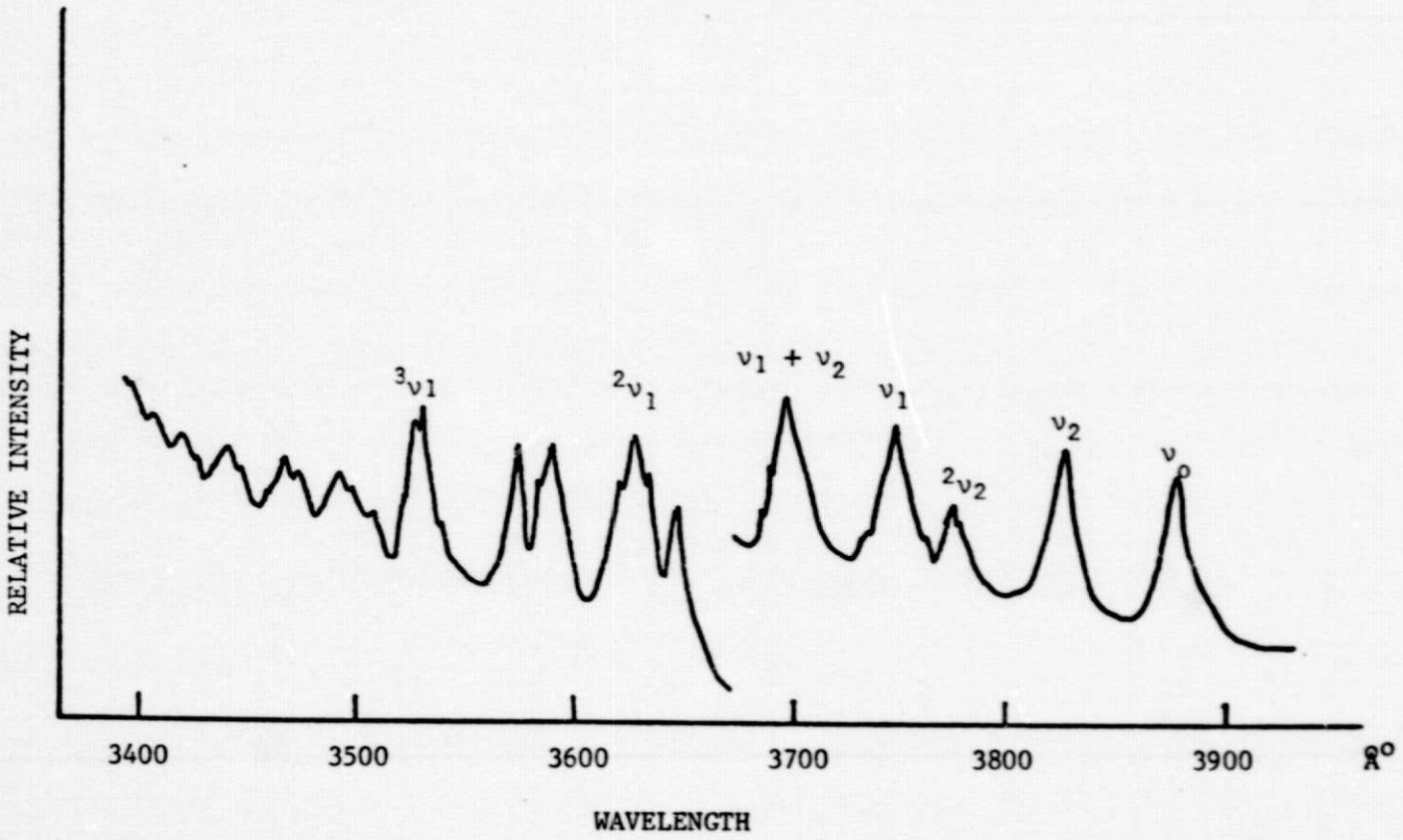

* J. D. Brand et. al., J. Mol. Spec. 45 404 (1973)

FIGURE 2

ELECTRONIC ABSORPTION OF N_2O AT 2595-3065Å *

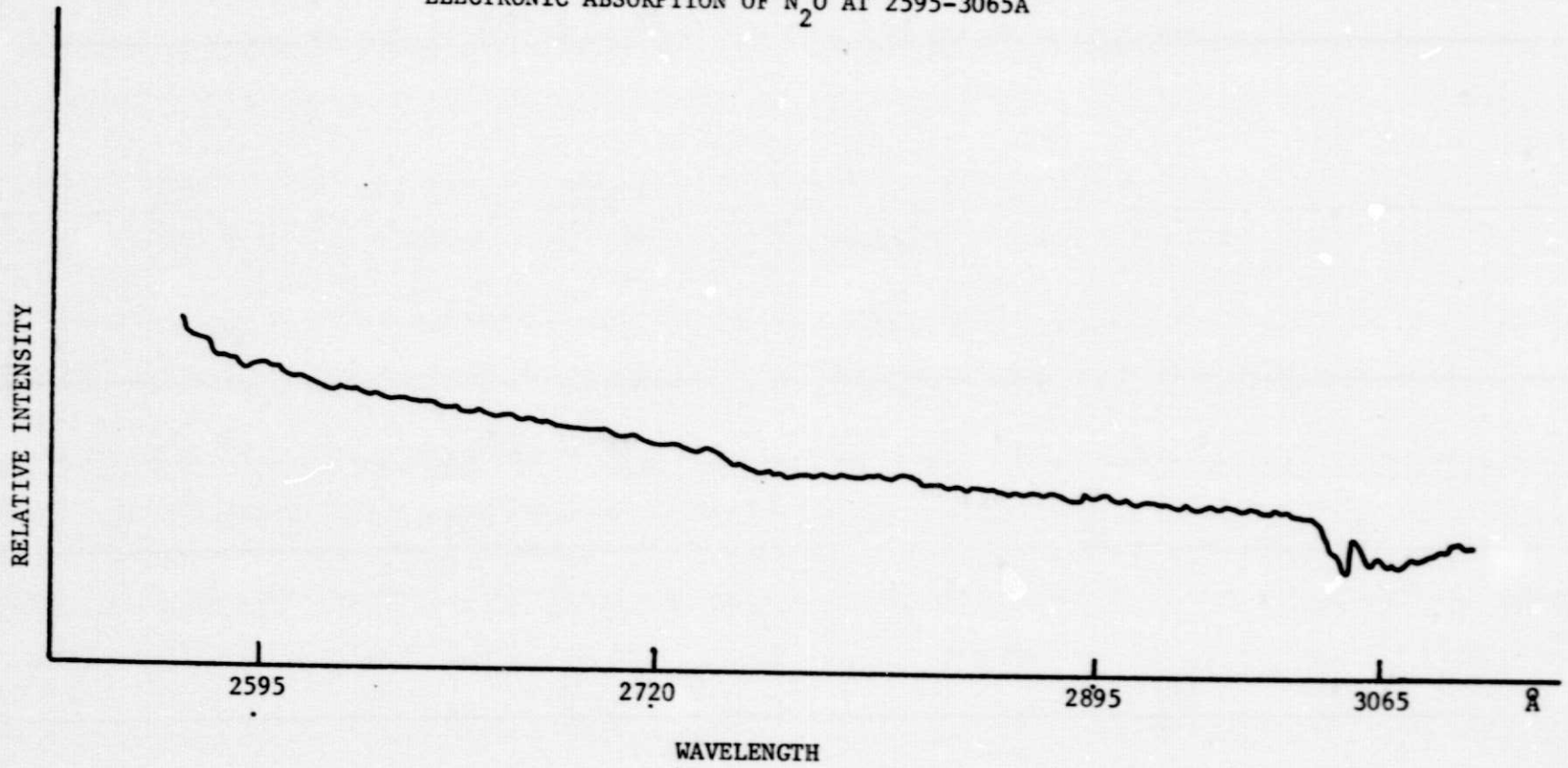

* H. Sponer and L. G. Bonner, J. Chem. Phys. 8 33 (1940)

FIGURE 3

ELECTRONIC ABSORPTION OF H_2S AT 1600-2100Å *

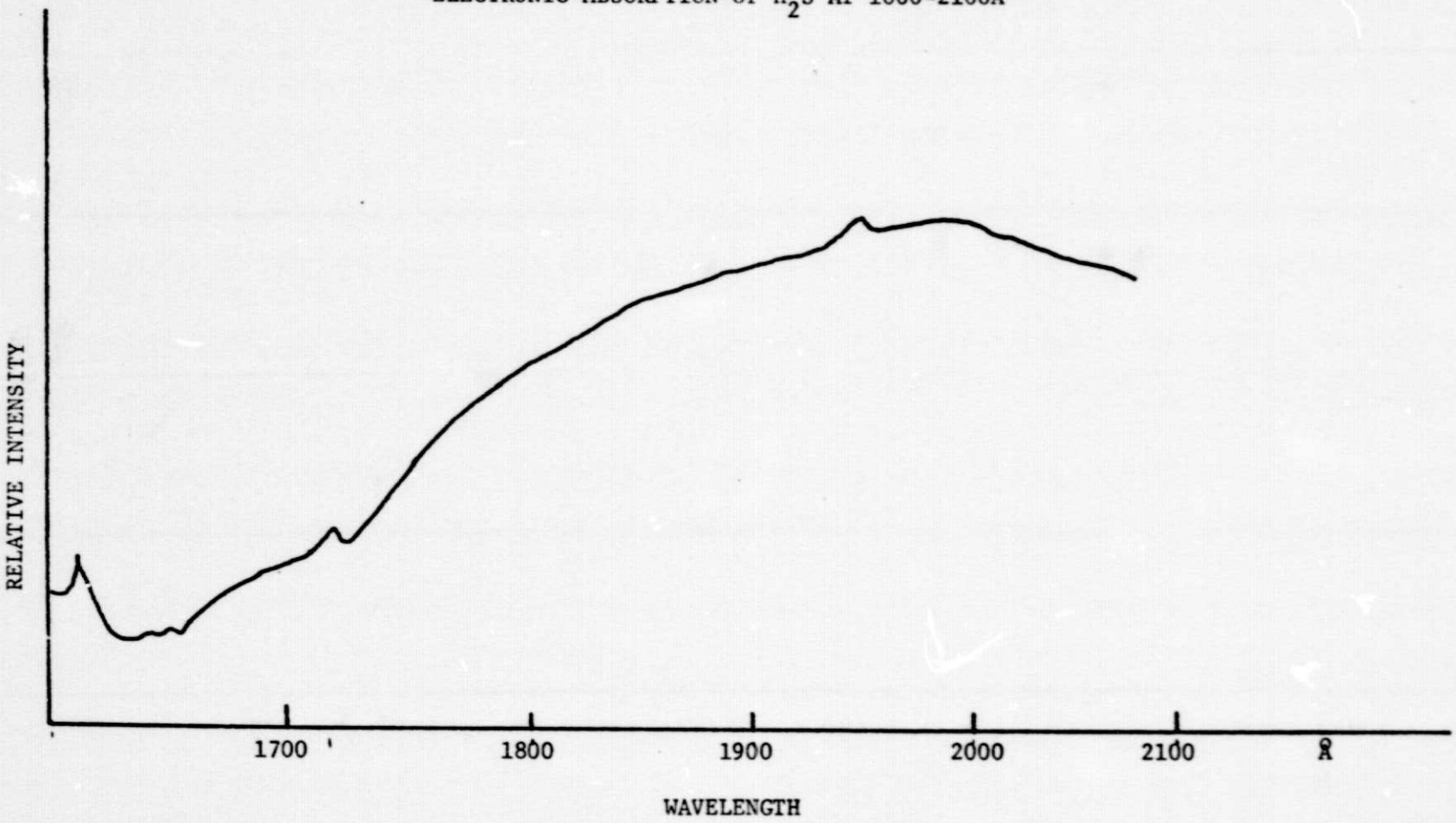

* K. Watanabe and A. S. Jursa, J. Chem. Phys. 41 1650 (1964)

FIGURE 4

SCHEMATIC DIAGRAM OF THE EXPERIMENTAL OPTICAL SYSTEM

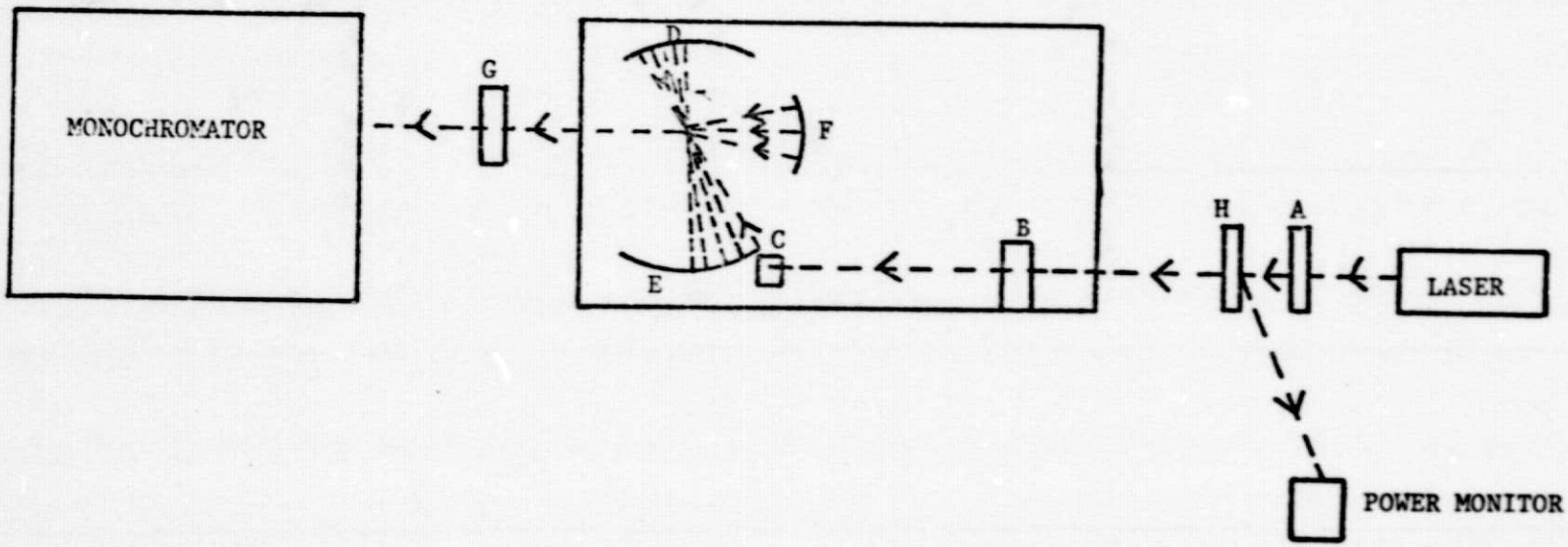

FIGURE 5

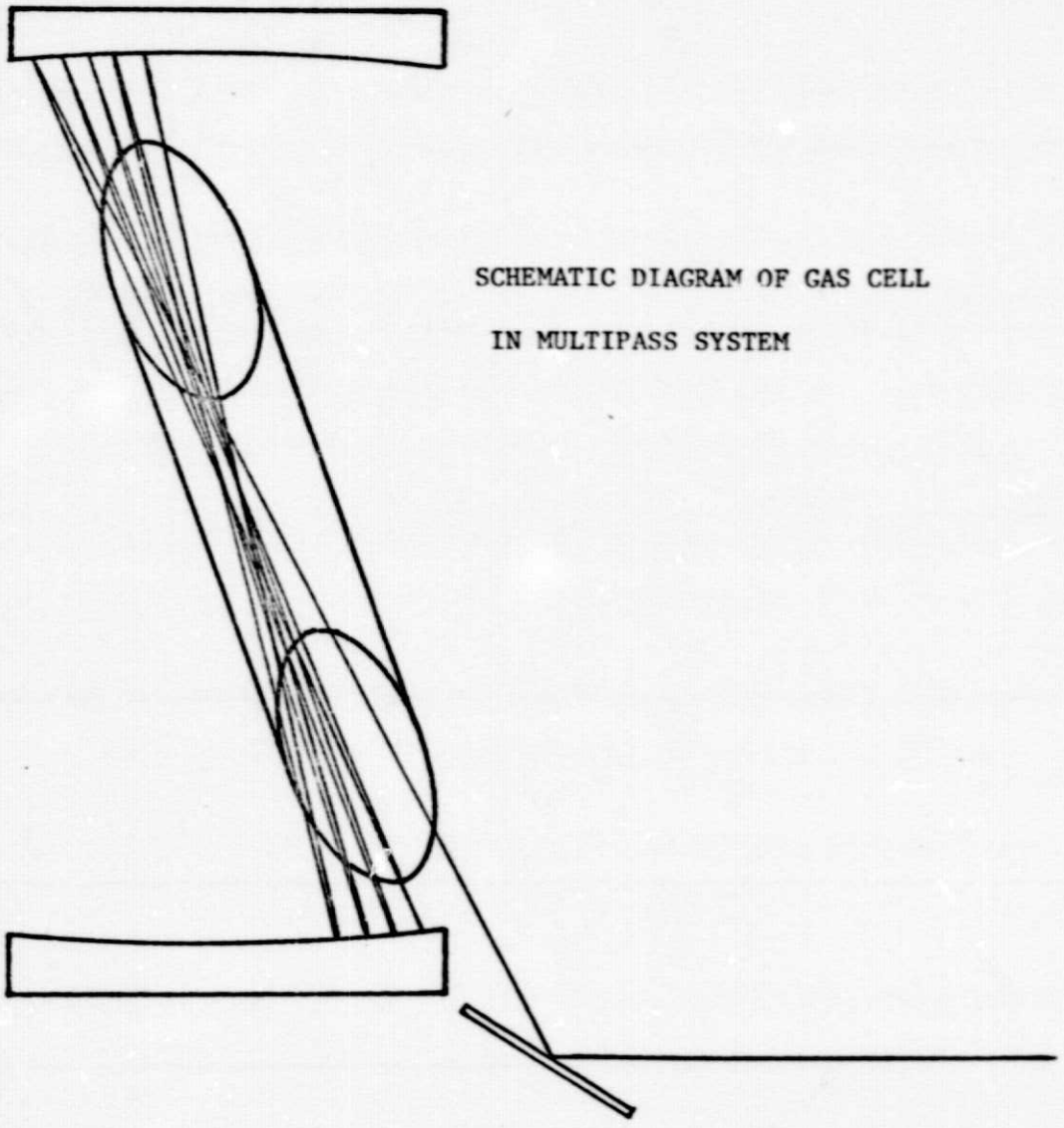

SCHEMATIC DIAGRAM OF GAS CELL

IN MULTIPASS SYSTEM

FIGURE 6

SCHEMATIC DIAGRAM OF THE GAS HANDLING SYSTEM

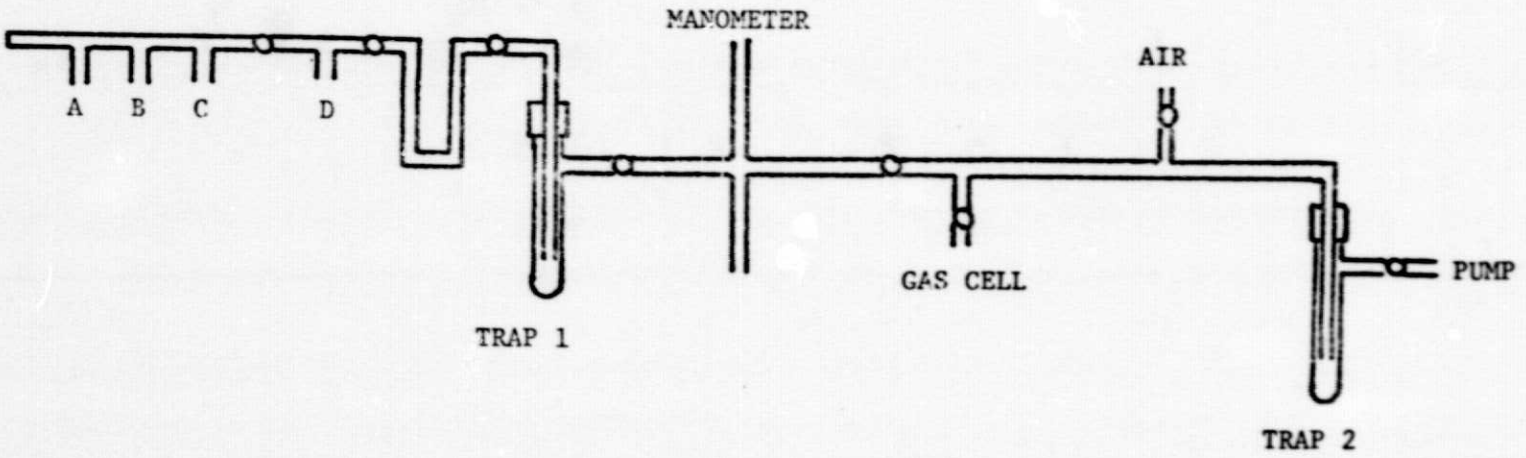

FIGURE 7

CALIBRATION CURVE OF OPTICAL SYSTEM EFFICIENCY AS A FUNCTION OF WAVELENGTH FOR 4880Å EXCITATION

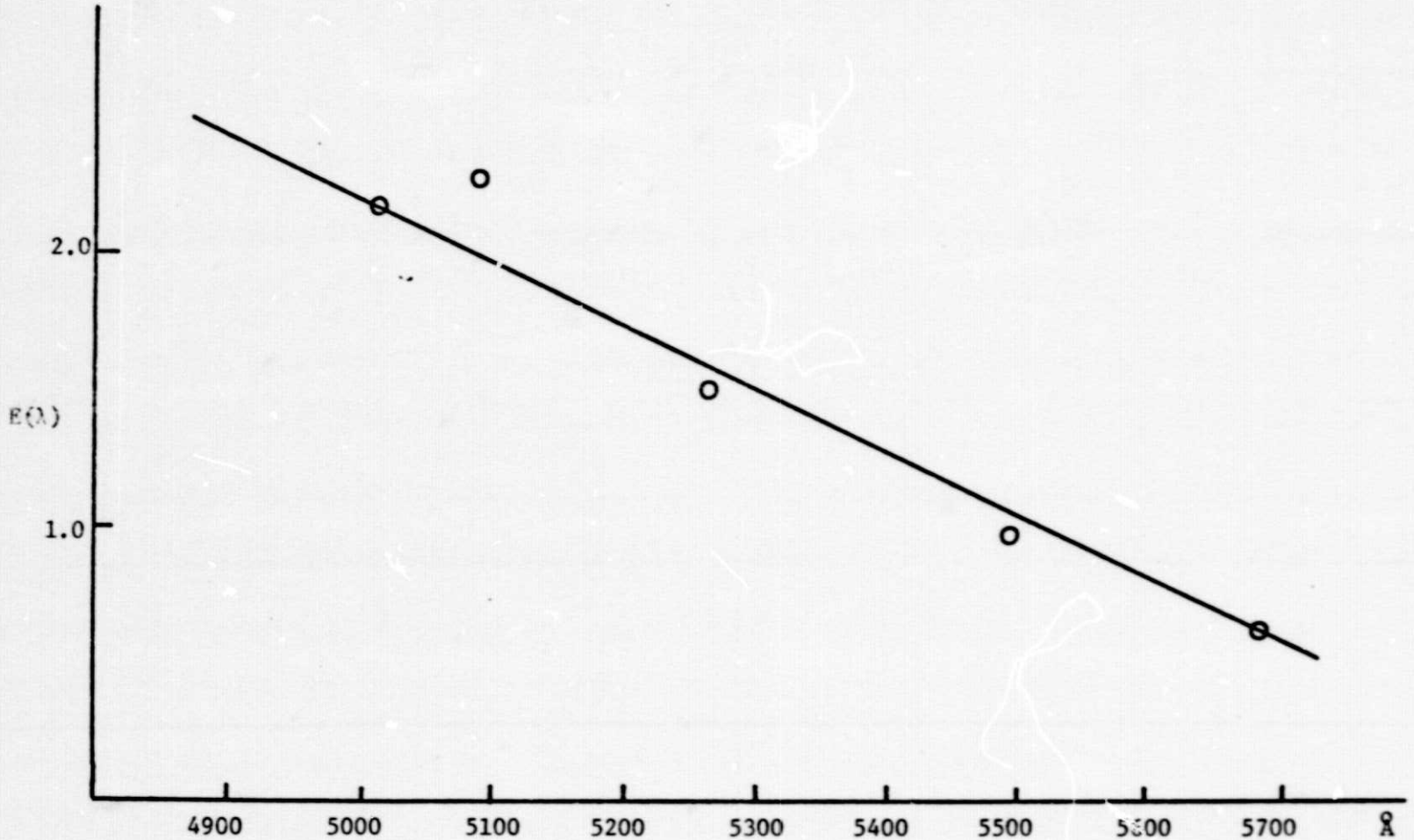

FIGURE 8

CALIBRATION CURVE OF OPTICAL SYSTEM EFFICIENCY AS A FUNCTION OF WAVELENGTH FOR 4727Å EXCITATION

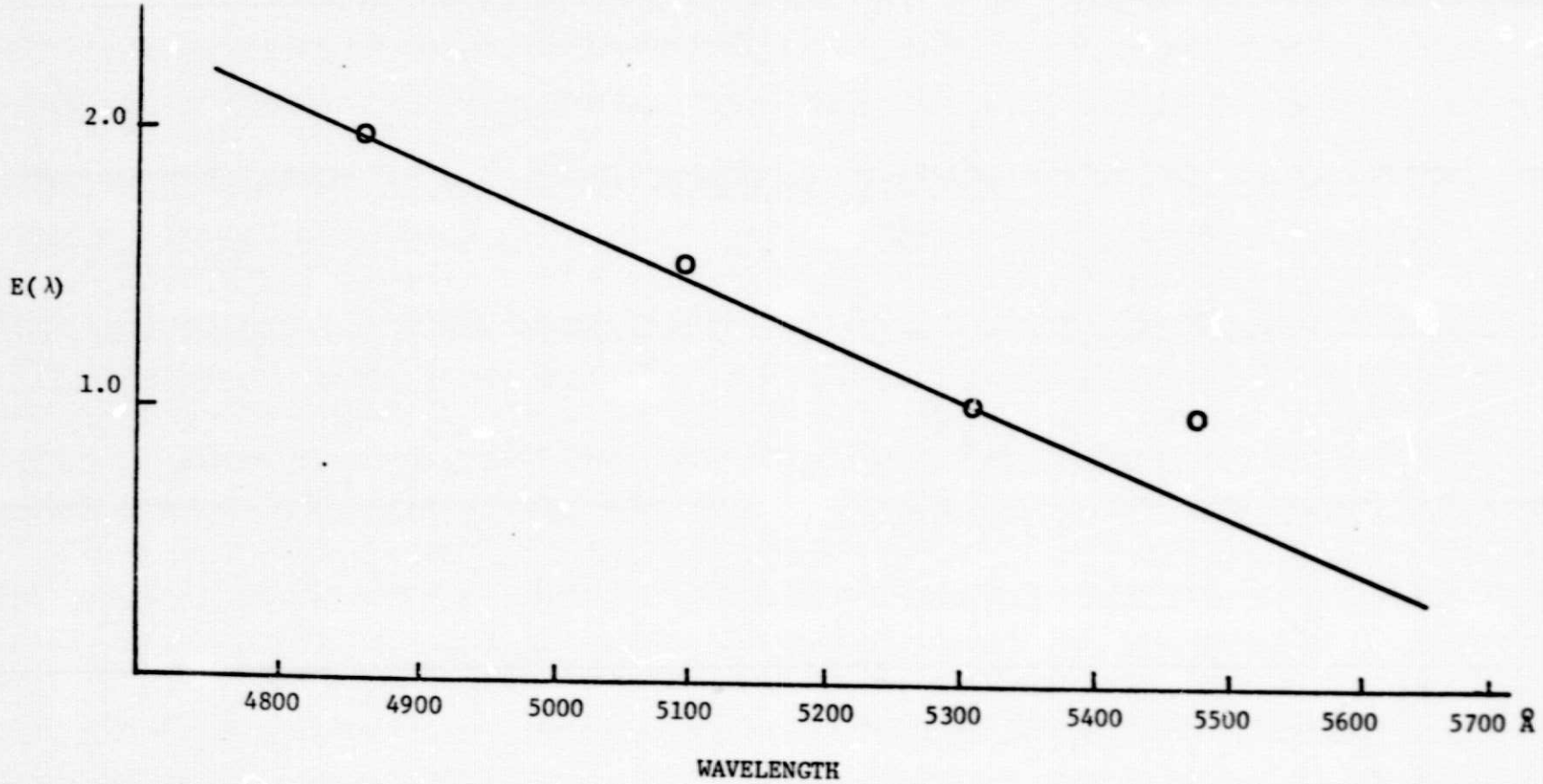

FIGURE 9

CALIBRATION CURVE OF OPTICAL SYSTEM EFFICIENCY AS A FUNCTION OF WAVELENGTH FOR 4579Å EXCITATION

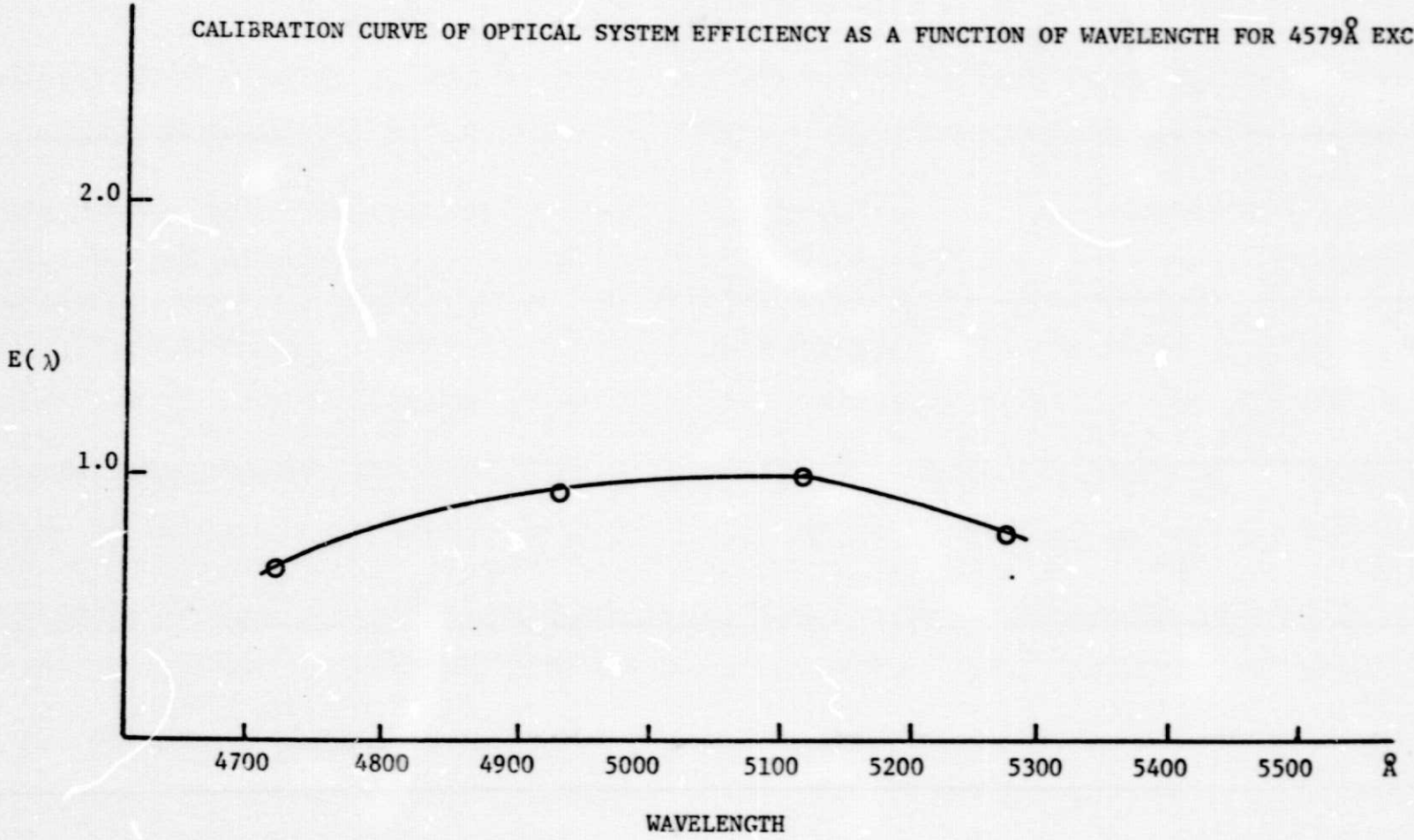

FIGURE 10

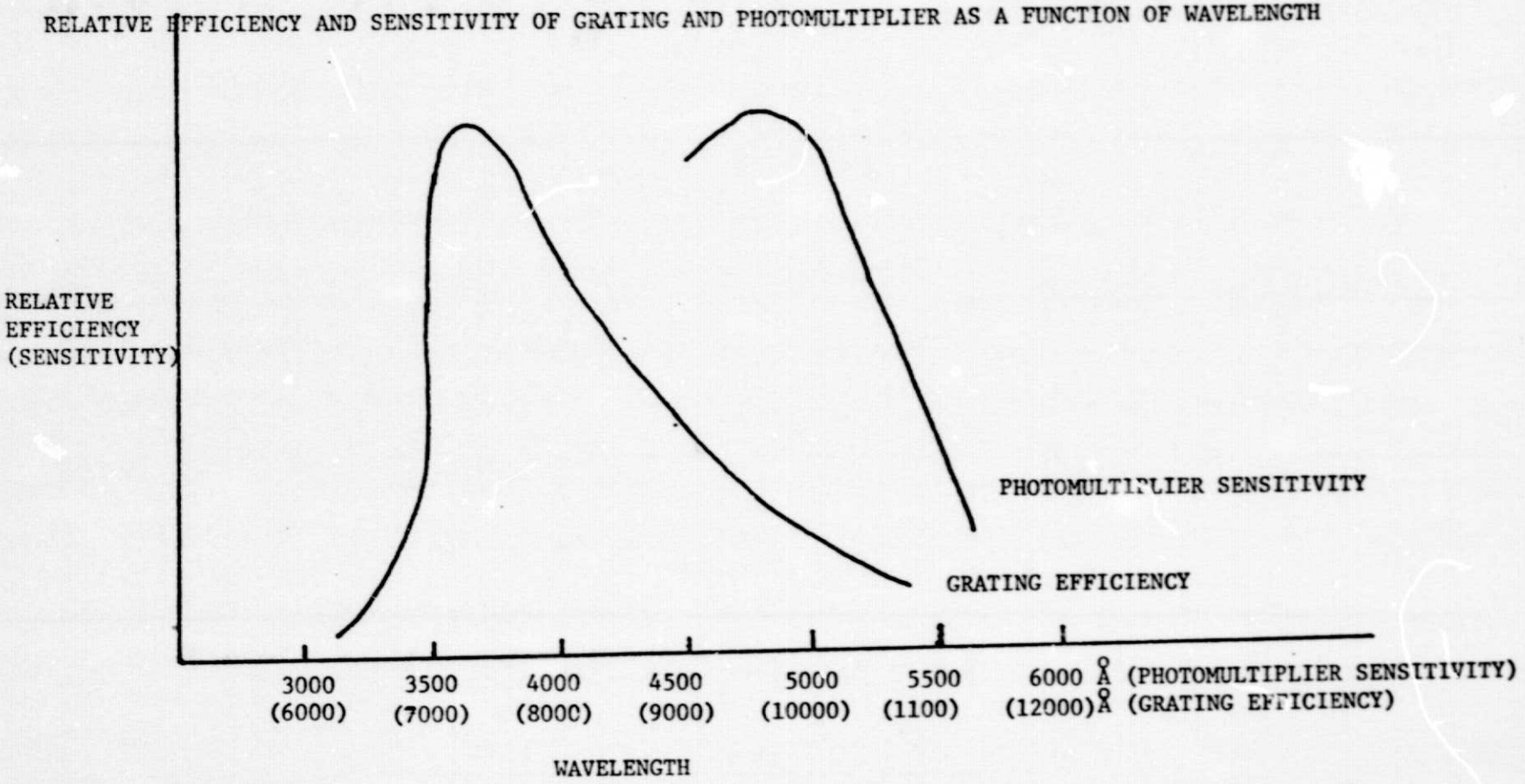
RELATIVE EFFICIENCY AND SENSITIVITY OF GRATING AND PHOTOMULTIPLIER AS A FUNCTION OF WAVELENGTH
RELATIVE EFFICIENCY (SENSITIVITY)
PHOTOMULTIPLIER SENSITIVITY
GRATING EFFICIENCY
3000 (6000)
3500 (7000)
4000 (8000)
4500 (9000)
5000 (10000)
5500 (1100)
6000 Å (12000) Å
(PHOTOMULTIPLIER SENSITIVITY)
(GRATING EFFICIENCY)
WAVELENGTH

TABLE 1

Experimental Cross Sections

Gas	4880Å	σ_g/σ_{N_2}	4727Å	σ_g/σ_{N_2}	4579Å	σ_g/σ_{N_2}	4880Å Literature Values of σ_g/σ_{N_2}
N_2	6.748×10^{-31}*	1	7.789×10^{-31}	1	8.984×10^{-31}	1	
N_2O	12.764×10^{-31}	1.89	15.477×10^{-31}	1.99	17.377×10^{-31}	1.94	(2.2) (2.7)
H_2S	46.813×10^{-31}	6.94	53.748×10^{-31}	6.90	54.310×10^{-31}	6.05	(6.6) (6.4)
SO_2	34.251×10^{-31}	5.08	33.158×10^{-31}	4.26	50.374×10^{-31}	5.61	(5.2) (5.5) (5.4)

*units are cm^2/ster.-mol. **see J. D. Brand, et.al., J. Mol. Spec.45, 404 (1973)

TABLE 2

Calculation of $\nu_{eg} - \nu_o$

H_2S*	N_2O	SO_2	Cl_2**
47, 619cm^{-1}	32,626cm^{-1}	25,773cm^{-1}	22,222cm^{-1}
25,780cm^{-1}	10,787cm^{-1}	3,934cm^{-1}	1,236cm^{-1}

*excitation 4579Å for all except Cl_2

**excitation for Cl_2 4765Å

TABLE 3

C_{2v} SYMMETRY GROUP

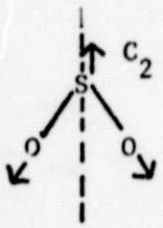

ν_1 (a_1) 1151 cm^{-1}

|| band α_{zz}, α_{yy}, α_{xx}

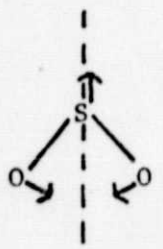

ν_2 (a_1) 517 cm^{-1}

|| band α_{zz}, α_{yy}, α_{xx}

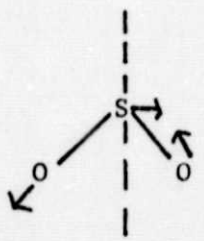

ν_3 (b_1) 1361 cm^{-1}

$\perp$ band α_{xz}

The electronic transition $^3B_1 \longleftarrow {}^1A_1$ is a $\perp$ band.

The transition moment is $|\mu_x|$

TABLE 4

Ratios of Experimental Cross Sections and Ratios of ν^4

Molecule	$4579\text{Å}/4880\text{Å}$	$\nu^4_{4579\text{Å}}/\nu^4_{4880\text{Å}}$	Deviation
SO_2	1.471	1.31	+0.161
N_2O	1.31	1.36	-0.05
H_2S	1.34	1.16	+0.18

TABLE 5

Equations (53) and (54) for SO_2

Equation	Frequency Factor	$I_{mn4579\text{Å}}/I_{mn4880\text{Å}}$
Equation (53)	$(\nu_o-\nu)^4/(\nu^2_{eg}-\nu^2_o)^2$	2.226
Equation (54)	$(\nu_o-\nu)^4(\nu^2_{eg}+\nu^2_o)^2/(\nu^2_{eg}-\nu^2_o)^4$	5.577

APPENDIX

DIFFICULTIES OF THE ULTRAVIOLET EXPERIMENT

Originally, this experiment was to include excitation with the two ultraviolet laser lines (3638Å and 3511Å) available in the argon ion laser. This part of the experiment presented immense difficulties. Most of these were eventually solved, and only the low power of the ultraviolet lines of the laser tube prevented conclusion of this part of the experiment. This appendix has been included in the belief that a discussion of the difficulties which were encountered and overcome might have some value to future experimentalists.

Although the laser was purchased with an ultraviolet option which makes available the power supply required to form the Ar^{2+} ion, and the mirrors necessary for these wavelengths, the actual power of the ultraviolet laser lines remained much too low. Atmospheric water vapor trapped in the dust shields was found to be the principal cause of the low power. The water vapor was removed by adding electrostatic precipitators to the laser. This modification increased the power to specifications level. However, water vapor and particles in the air external to the laser cavity also presented a problem, since they could absorb or scatter the ultraviolet radiation and reduce the power reaching the sample. This loss was reduced to an acceptable level by changing the experimental configuration of the entire optical system to make the path the laser line travelled as short as possible. Although these refinements raised the laser power reaching the sample chamber to an acceptable level, the power in the sample chamber itself remained too low. The mirrors absorbed rather than reflected the

laser beam. (The coatings on the reflecting mirrors were found to be improper for use with ultraviolet radiation.) After the mirrors were properly coated, the laser power was sufficient in the sample region to obtain a Raman signal.

In an attempt to get Raman spectra the problems of fluorescence and Mie scattering became apparent. These two phenomena resulted in excessively high background and large Mie scattering peaks. The initial quartz gas sample cell fluoresced, and was replaced with one made from fluorescence-free quartz. With the new cell, the background decreased considerably. The Mie scattering was predominately a result of plasma radiation from the laser. Plasma radiation, while also present with the visible lines, presented a very special problem when using the ultraviolet lines, since the power of the ultraviolet lines was so much less than the visible lines. The scattering from the plasma radiation can be as intense as Raman scattering from the excitation lines. The plasma radiation was reduced by placing a stop just before the laser lines enter the multipass system. (See Figure 4.) Since the plasma radiation is not coherent it radiates as ordinary light; thus the farther from the source the more diffuse it becomes and greater is the percentage which can be removed by a stop. This addition proved to be an extremely successful method for removing the background and Mie scattering peaks. Unfortunately, after all the experimental difficulties seemed to be overcome, the laser tube had to be replaced, and the new tube had insufficient power in the ultraviolet lines to complete the experiment.

LITERATURE CITED

1. Behringer, Josef, "Observed Raman Spectra," Raman Spectroscopy, Szymanski, H., ed, New York, Plenum Press, 1967.
2. Holzer, W., W.F. Murphy, and H.J. Bernstein, J. Chem Phys. 52, 399 (1970)
3. Kiefer, W. and H.J. Bernstein, J. Chem. Phys. 43, 366 (1972)
4. Gillespie, R.J. and M.J. Morton, J. Mol. Spec 30, 178 (1969)
5. Maier, Werner and Frederich Dorr, Appl.Spec. 14, 1 (1960)
6. Brand, J.C.D. V.T. Jones, and C. DiLauro, J. Mol. Spec. 40, 616 (1971)
7. ibid., 45, 404 (1973)
8. Brand, J.C.D. and R. Nanes, J. Mol. Spec. 46, 194 (1973)
9. Merer, A.J., Disc. Faraday Soc.1963, 127 (1963)
10. Sponer, H. and L.G. Bonner, J. Chem. Phys. 8, 33 (1940)
11. Walanabe, K. and A.S. Juisa, J. Chem. Phys. 41, 1650 (1964)
12. Shorygin, P.P., Izv. Akad. Nauk. S.S.S.R. Ser. Fiz. 17, 581 (1953)
13. Krushenskii, L.L. and P.P. Shorygin, Doklady Akad. Nauk. S.S.S.R. 133, 337 (1960)
14. Albrecht, Andreas C., J. Chem. Phys. 34, 1476 (1960)
15. Lang, J. and A.C. Albrecht, J. Chem. Phys. 49, 1144 (1968)
16. Murphy, W.F., W. Holzer, and H.J. Bernstein, Appl. Spec. 23, 211 (1969)
17. Fenner, W.R., H.A. Hyatt, J.M. Kellam, and S.P.S. Porto, J. Opt. Soc. Amer. 63, 73 (1973)
18. Koningstein, J. A., Introduction to the Theory of the Raman Effect, Dordrecht-Holland, D. Reidel Publishing Company, 1972.